## Measuring nanoscale thermal gradients in suspended MoS<sub>2</sub> with STEM-EELS

Cite as: Appl. Phys. Lett. 115, 153108 (2019); https://doi.org/10.1063/1.5094443 Submitted: 01 March 2019 . Accepted: 28 July 2019 . Published Online: 09 October 2019

Lang Shen 🗓, Matthew Mecklenburg 🗓, Rohan Dhall, B. C. Regan, and Stephen B. Cronin 🗓



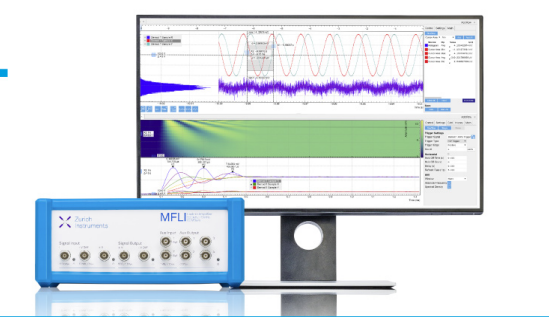




Challenge us. What are your needs for periodic signal detection?









## Measuring nanoscale thermal gradients in suspended MoS<sub>2</sub> with STEM-EELS

Cite as: Appl. Phys. Lett. 115, 153108 (2019); doi: 10.1063/1.5094443 Submitted: 1 March 2019 · Accepted: 28 July 2019 ·

Published Online: 9 October 2019









Lang Shen,<sup>1,a)</sup> (b) Matthew Mecklenburg,<sup>2,a),b)</sup> (b) Rohan Dhall,<sup>3</sup> B. C. Regan,<sup>4</sup> and Stephen B. Cronin<sup>5</sup> (b)







- $^1$ Mork Family Department of Chemical Engineering and Materials Science, University of Southern California, Los Angeles, California 90089, USA
- <sup>2</sup>Core Center of Excellence in Nano Imaging (CNI), University of Southern California, Los Angeles, California 90089, USA
- <sup>3</sup>National Center for Electron Microscopy (NCEM), Molecular Foundry, Lawrence Berkeley National Laboratory, California, 94720, USA
- <sup>4</sup>Department of Physics and Astronomy, University of California, Los Angeles, California, 90095, USA
- <sup>5</sup>Ming Hsieh Department of Electrical Engineering, University of Southern California, Los Angeles, California 90089, USA
- a) Contributions: L. Shen and M. Mecklenburg contributed equally to this work.
- b) Author to whom correspondence should be addressed: matthew.mecklenburg@usc.edu

## ABSTRACT

Transition metal dichalcogenides such as molybdenum disulfide (MoS<sub>2</sub>) may see service in the heart of next-generation nanoelectronic devices, where highly localized power dissipation can produce nontrivial temperature gradients over nanometer-scale distances. Here, we demonstrate that MoS2 is a promising target for plasmon energy expansion thermometry (PEET), a high-spatial resolution temperature mapping technique employed in a scanning transmission electron microscope (STEM) equipped with electron energy loss spectroscopy (EELS). We first use a calibrated, commercial MEMS-style TEM sample heater chip to measure the temperature dependence of the MoS<sub>2</sub> bulk plasmon. We corroborate the chip's temperature calibration with Raman thermometry and determine the bulk thermal expansion coefficient (TEC) of MoS<sub>2</sub> in the temperature range of 300-1100 K. Applying this TEC value to PEET measurements on a suspended MoS<sub>2</sub> flake, we map 70–90 K/ $\mu$ m temperature gradients with a submicrometer spatial resolution.

Published under license by AIP Publishing. https://doi.org/10.1063/1.5094443

Transition metal dichalcogenides (TMDCs) draw attention because their weak out-of-plane bonding enables easy isolation of their atomically thin constituents. Their extraordinary electrical and optical properties and mechanical flexibility make TMDCs excellent candidates for novel nanoscale electronic and optoelectronic devices. As device features approach or reach the atomic limit,2 nanometer-scale thermometry techniques are required to better understand their thermal transport and heat management.

The currently available temperature measurement techniques with submicrometer resolution are generally optical-3,4 or scanning probebased.<sup>5,6</sup> Optical techniques (e.g., Raman, infrared detection) are noncontact, but diffraction limits their resolution to several hundred nanometers. Scanning probe techniques achieve ~10 nm resolution, but thermal contact requires perturbing the probed small volumes' temperature, introducing errors that are challenging to estimate and control.

Plasmon energy expansion thermometry (PEET) is a noncontact, nanoscale temperature mapping technique based on electron energy loss spectroscopy (EELS) in a scanning transmission electron microscope (STEM).<sup>8,9</sup> This approach exploits the temperature dependence of a material's bulk plasmon energy: thermal expansion or contraction changes the local electron density, which, in turn, shifts the bulk plasmon energy. In PEET, a STEM equipped with EELS rasters a focused probe across the sample and collects a spectrum at each beam position (the 3D data array is called a spectrum image). Analyzing a spectrum image produces a plasmon energy map, which is subsequently converted into a temperature map, using the material's known thermal expansion coefficient (TEC). For materials with sufficiently sharp plasmon resonances, PEET provides a method for obtaining temperature maps with a nanometer-scale resolution.

Other TEM-based temperature measurements use diffractionbased detection of thermal expansion, <sup>10</sup> detailed balance using EELS, <sup>11</sup> or thermal population of Stokes/anti-Stokes excitations. 12 The phononbased measurements are a novel and more fundamental means to measure temperature, but phonons are more delocalized than plasmons. So far, temperature gradients in the TEM have only been observed with PEET, although other techniques have such potential.

In the work presented here, we apply PEET to the prototypical member of the TMDC family, molybdenum disulfide (MoS<sub>2</sub>). We use an FEI NanoEx<sup>TM</sup>-i/v TEM microheater chip <sup>13</sup> [Fig. 1(a)] with a vendor-supplied calibration of temperature-vs-microheater resistance. Depositing a MoS<sub>2</sub> flake, we corroborate the vendor calibration using both conventional (diffraction limited) Raman thermometry and PEET. Finally, we use a homemade microheater chip [Fig. 1(b)] to create switchable, opposing, nanoscale temperature gradients across a MoS<sub>2</sub> flake that we map using PEET.

Few layer MoS<sub>2</sub> flakes are dry-transferred via mechanical exfoliation (scotch tape method) to a commercial or homemade TEM chip (Fig. 1),<sup>14</sup> avoiding some wet transfer contamination.<sup>15</sup> The MoS<sub>2</sub> is exfoliated first from the bulk material (SPI Supplies, Inc.) onto a transparent polydimethylsiloxane (PDMS) substrate, and

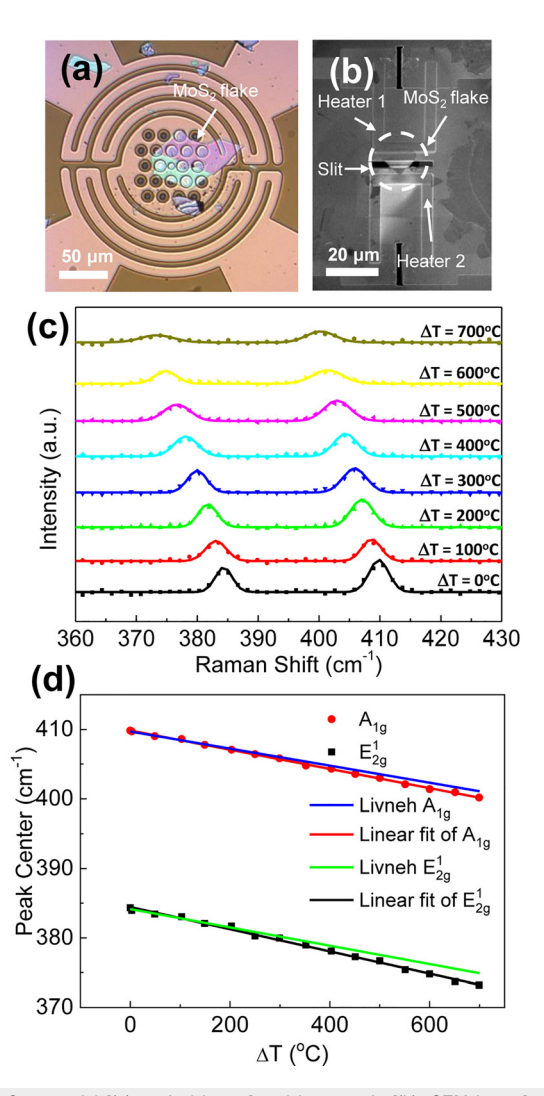


**FIG. 1.** Commercial [(a), optical image] and homemade [(b), SEM image] microheater chips with MoS $_2$  flakes deposited. (c) Raman spectra of MoS $_2$  at different temperatures. (d) Comparison of theoretical and experimental Raman peak positions as a function of temperature change ( $\Delta T$ ). In (d) the offsets were kept the same [from the value determined in (c)] and the different slopes are plotted.

then a thick flake ( $\gtrsim$ 10 layers) is located using optical microscopy. <sup>16</sup> The target flake is transferred to the TEM chip using a home-built contact aligner. <sup>17</sup> The chips are wire bonded to PCB chip carriers customized for a TEM biasing holder (Hummingbird, Inc.), and electrical power is supplied by a Keithley 2400 Sourcemeter controlled with LabVIEW.

For Raman thermometry, the samples are placed in a cryostat (Cryo Industries, Inc.) with a base pressure of  $<\!10^{-5}\,\rm Torr.$  Raman spectra are collected using a Renishaw InVia confocal Raman microscope with  $100\,\mu\rm W$  of a 532 nm laser excitation. TEM data are acquired in a JEOL JEM-2100F with a Gatan Quantum 963 GIF. Standard temperature mapping conditions used an 80 kV accelerating potential, a beam current of 0.3 nA, and a 12–14 mrad beam convergence semiangle (19–22 mrad spectrometer collection semiangle). PEET mapping conditions use a beam current of 0.3 nA, a 12–14 mrad beam convergence semiangle, a 19–22 mrad spectrometer collection semiangle, and a 0.025 eV/bin EELS dispersion. The calibrated heater experiment is performed with an accelerating potential of 200 kV and an EELS zero-loss peak (ZLP) full-width at half maximum (FWHM) of 0.95 eV, while the gradient experiment is performed with 80 kV and a ZLP FWHM of 0.65 eV.

Raman spectroscopy is a noncontact, nondestructive technique widely used to study mechanical and thermal properties of graphene and TMDCs. Raman peak positions shift and broaden with increasing temperature and have been measured for vapor-phase-grown, exfoliated, and hydrothermal-synthesized MoS<sub>2</sub> flakes. The in-plane mode  $\rm E^1_{2g}$  and out-of-plane mode  $\rm A_{1g}$  frequencies show a linear variation with temperature. This temperature dependence can be mapped with  $\sim \! 1 \, \mu \rm m$  spatial resolution. Moreover, the temperature variation of these Raman frequencies is primarily due to thermal expansion. Thus, the shifting of Raman peaks and bulk plasmon peaks is similar, making Raman thermometry, which is comparatively well-established, an appropriate technique for calibrating temperature measurements in MoS<sub>2</sub> via PEET.

Figure 1 shows the NanoEx chip with a  ${\sim}20\,\text{nm}\text{-thick MoS}_2$  flake and the shifts of the MoS $_2$  E $^1_{2g}$  and  $A_{1g}$  Raman modes at elevated temperatures. Temperatures are determined from the calibrated heater resistance. Linear fitting gives first order temperature coefficients of  $\gamma(E^1_{2g})=-1.60\pm0.03\times10^{-2}\,\text{cm}^{-1}/\text{K}$  and  $\gamma(A_{1g})=-1.39\pm0.01\times10^{-2}\,\text{cm}^{-1}/\text{K}$ . We observe reasonable agreement ( ${\sim}10\%$ ) with the linear dependence reported by Livneh  $\it{et~al.},\,\gamma(E^1_{2g})=-1.47\times10^{-2}\,\text{cm}^{-1}/\text{K}$  and  $\gamma(A_{1g})=-1.23\times10^{-2}\,\text{cm}^{-1}/\text{K}$ , shown as green  $(E^1_{2g})$  and blue  $(A_{1g})$  lines in Fig. 1(d).  $^{20,21}$ 

After confirming the  $MoS_2$  flake temperature via Raman thermometry, we switch to plasmon thermometry. EELS spectra (5 of 29) of suspended  $MoS_2$  at different temperatures are shown in Fig. 2(a). The plasmon peak's maximum shift is equivalent to just seven spectrometer bins in the 2048-bin spectrum. Spectrum images are acquired at different temperatures, and the plasmon energy shifts are determined by fitting the ZLP and the  $MoS_2$  plasmon peak with Gaussian and Lorentzian functions, respectively. The measured bulk plasmon energy of  $MoS_2$  is defined as the difference between the ZLP's and  $MoS_2$  plasmon peak's fitted centers, eliminating common-mode effects caused by the beam shifting relative to the spectrometer.

The curve fit spectrum images produce plasmon energy maps showing a clear systematic shift with temperature (supplementary material, Fig. 1). Each map produces a normally distributed set of plasmon energies

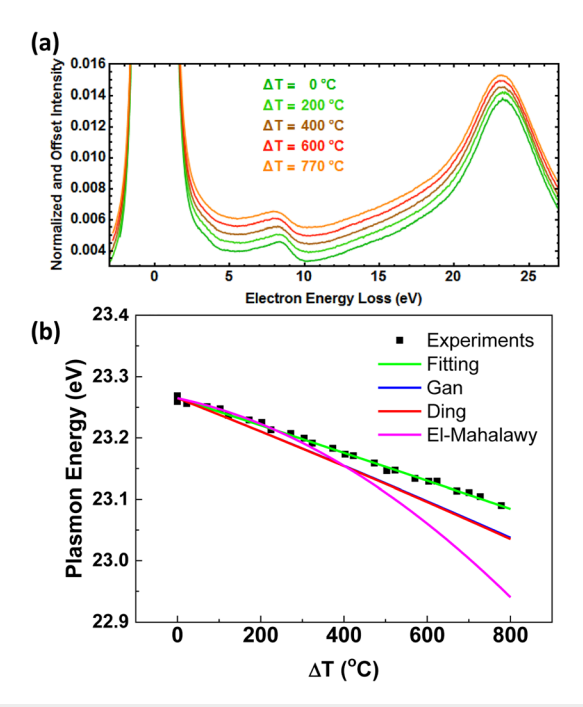


**FIG. 2.** (a) A sampling (5 of 29) of EELS spectra over a range of temperatures in the heating experiment. The spectra are offset vertically for clarity. (b) Comparison of theoretical and experimental plasmon energy shifts as a function of temperature change ( $\Delta T$ ).

per temperature (supplementary material, Fig. 1), from which a mean and standard deviation are extracted.

According to the electron gas model, the bulk plasmon energy  $E_p = \hbar \omega_p = \hbar \sqrt{4\pi n e^2/m}$ . At elevated temperatures, the valence electron number density n in the  $MoS_2$  decreases due to thermal expansion according to the relation  $n(T) \approx n(T_0) |1 - f(T)|$ , where  $f(T) = \int_{T_0}^T \alpha_V(T') dT' \approx \alpha_1 \Delta T + \alpha_2 \Delta T^2$ , and  $\alpha_1$  and  $\alpha_2$  are the first and second order volume (not to be confused with linear) TECs, respectively.<sup>22–24</sup> Temperature changes  $\Delta T = T - T_0$  are measured relative to a reference temperature, here taken to be room temperature ≡ 300 K. Combining the equations for  $E_p$  and n(T) gives the bulk plasmon energy as a function of temperature,  $E_p(T) \simeq E_p(T_0)[1]$  $-\frac{1}{2}f(T)$ ] =  $E_p(T_0)$  $\left[1-\frac{1}{2}(\alpha_1\Delta T+\alpha_2\Delta T^2)\right]$ . Figure 2(b) shows, as a function of temperature change  $\Delta T$ , the measured bulk plasmon energies, along with predictions of  $E_p$  and reported  $\alpha_V$  values<sup>25,26</sup> for comparison. Fitting the experimental values to a second order polynomial [green line in Fig. 2(b)] gives the estimates  $\alpha_1 = 1.9 \pm 0.1 \times 10^{-5} \, \text{K}^{-1}$  and  $\alpha_2 = 5 \pm 8 \times 10^{-10} \,\mathrm{K}^{-2}$  in the range of 300–1100 K.

The literature values for the TECs of MoS<sub>2</sub> are various and confusing. In the 1970s, El-Malahaway and Evans, <sup>26</sup> and Murray and the same Evans, <sup>27</sup> measured MoS<sub>2</sub>'s lattice parameters in the temperature ranges of 20–850 °C and 10–320 K, respectively, using X-ray diffraction. Unfortunately, while the data are consistent in the overlap region, the lattice-constant fit parameters (from which the TECs are extracted) given by Murray and Evans, do not match their own data. Moreover, the low-temperature TECs in Ref. 27 are more than twice than the high-temperature TECs in Ref. 26, which is unphysical since TECs are expected to approach zero in the low-temperature limit. A more recent

theory by Ding and Xiao<sup>25</sup> and Gan and Liu<sup>28</sup> matches this expectation, indicating that the MoS<sub>2</sub> TEC increases rapidly from zero below room temperature and then more slowly above room temperature. In quoting the X-ray data for comparisons, however, these<sup>25,28</sup> and other authors<sup>29</sup> note neither Murray and Evan's error nor that the high-temperature TECs<sup>26</sup> are referenced to 0 °C and the low-temperature TECs<sup>27</sup> to 0 K, where, by all accounts, the TEC is very different. Huang and Zeng<sup>30</sup> and Hu *et al.*<sup>29</sup> have studied the in-plane thermal expansion of single and few-layer MoS<sub>2</sub>. Hu *et al.* used shifts in the plasmon energy to measure in-plane thermal expansion coefficient values, but unfortunately do not give bulk volume TEC values (no out-of-plane component is given); so, a comparison is not possible.

Given this state of affairs, we ignore the TEC data of Murray and Evans entirely. Table I lists the other values available. The values of El-Mahalawy and Evans are outliers and thus seem implausible, not only because of the small value of  $\alpha_1$  but also because their (linearized) volume TEC increases by a factor of  $2\alpha_2\Delta T/\alpha_1 \sim 4$  over their measured temperature range of  $20-850\,^{\circ}$ C. For the other three entries (two of them theoretical), the corresponding increase is  $\leq 15\%$ . The value on the last line is the result of a quadratic fit of  $E_p(T)$  to the data [Fig. 2(b)], where the errors are statistical and reflect the scatter in the data plotted.

To determine Raman-based temperatures in MoS<sub>2</sub> flakes, we invert the equations describing the peak shift's temperature dependence. We have  $\Delta T_{Raman} = \left[\omega(T) - \omega(T_0)\right]/\gamma$ , where  $\omega$  is the frequency, and  $\gamma$  is the first order temperature coefficient, of the Raman mode. <sup>18</sup> In the case of PEET, we solve  $E_p(T)$  for  $\Delta T$ , finding

$$\Delta T_{PEET} = \frac{\alpha_1}{2\alpha_2} \left( \sqrt{1 - \frac{8R\alpha_2}{\alpha_1^2}} - 1 \right) \simeq -\frac{2R}{\alpha_1}$$

$$= -\frac{2}{\alpha_1} \frac{\omega_p(T) - \omega_p(T_0)}{\omega_p(T_0)}, \tag{1}$$

where the normalized change in the plasmon energy  $R \equiv [E_p(T) - E_p(T_0)]/E_p(T_0)$ . Here, we show the linear approximation to emphasize the similarity (the origin of the "2" is the square-root in the plasmon energy) with the Raman case. For the Raman-based determination of the  $\text{MoS}_2$  flake's temperature, only two Raman spectra are acquired: room temperature and an elevated temperature. In contrast, for the PEET-based temperature determination, R is obtained at each point from two spectrum *images*. Raman thermometry provides point measurements on the  $\mu$ m-scale, while PEET can provide nm-scale maps.

When normalized for the integration time, the statistical precision of Raman thermometry and PEET are comparable in MoS<sub>2</sub>. Raman spectra, acquired in 30 seconds, have a statistical uncertainty of

**TABLE I.** Comparison of the first and second order volume thermal expansion coefficients of MoS<sub>2</sub>.

Author $(T_0)$	$\alpha_1(10^{-5}K^{-1})$	$\alpha_2  (10^{-10}  \text{K}^{-2})$
El-Mahalawy and Evans <sup>26</sup> (273 K)	1.25	280
Ding and Xiao <sup>25</sup> (300 K)	2.3	21
Gan and Liu <sup>28</sup> (300 K)	2.3	18
Present work, EELS (300 K)	$1.9 \pm 0.1$	$5\pm8$

about 0.4 K (2 K/ $\sqrt{\text{Hz}}$ ). PEET spectra, acquired in 0.05 s, have a statistical uncertainty of about 12 K (3 K/ $\sqrt{\text{Hz}}$ , similar to aluminum in Ref. 8).

Plotting  $\Delta T_{PEET}$  and  $\Delta T_{Raman}$  vs the vendor-calibrated chip temperature  $\Delta T_{holder}$  (Fig. 3) shows that the Raman  $E_{2g}^1$  and  $A_{1g}$  peaks give values that are systematically +9% and +13% high, respectively. PEET values, calculated using the TEC values of Gan and Liu for illustration purposes, are systematically low by 22%. (The values in the last line of Table I would give perfect agreement by construction.) Clearly systematic errors dominate statistical errors in both Raman and PEET thermometry (their scatter is small). One possibility is that the chip calibration, specified to be good at 5%, is incorrect. The chip's heater/ thermometer could have been miscalibrated or altered, either during flake deposition or use. However, a different chip calibration would not make the Raman data agree with the PEET data. Thus, it appears that the temperature coefficients of the Raman modes, the available MoS<sub>2</sub> TEC values, the chip calibration, or some combination of these three are incorrect. Clearly, more work is required to demonstrate consistent and reproducible accuracy with these three thermometric techniques. On a more promising note, the lack of scatter in the data indicates that relative thermometry with precision at the few percent level is already possible. Because the Raman and the chip thermometries agree better than the other two pairs, we elect to take those values as more reliable and thus the value for MoS2's volume TEC given in the last line of Table I as the best available.

We now apply PEET to mapping a nanoscale temperature gradient in a suspended 30 nm-thick  $MoS_2$  flake. To create temperature gradients, we use a homemade chip [Figs. 1(b) and 4(a)], applying heater power alternately on one side or the other (the heater on the opposing side is grounded). Spectrum images are acquired with neither heater powered (reference temperature  $T_0$ ) and one heater powered (unknown temperature  $T_0$ ), aligned to remove spatial drifts, and fit to give the plasmon energies. With the aligned maps of plasmon energies, the normalized change R is calculated for each pixel and then converted to a temperature map.

Applying 100 mW to the two heaters alternately gives two temperature maps [Fig. 4(b)]. Averaging the mapped region along the

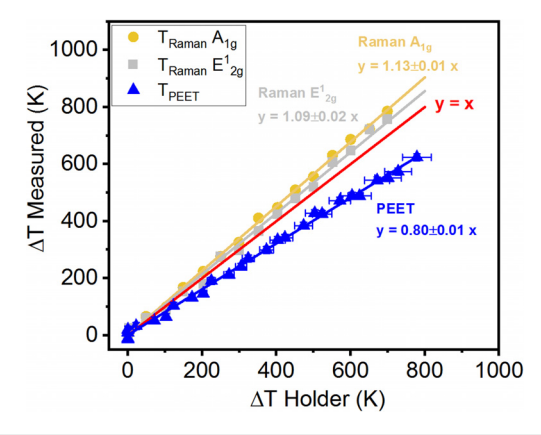


**FIG. 3.** Measured temperature changes ( $\Delta T$  measured) obtained from PEET and Raman measurements plotted as a function of chip temperature ( $\Delta T$  holder), with corresponding fits. The x-error bars are derived from the commercial MEMS chip vendor's specification of the accuracy of the heater/thermometer calibration (5%). The y-error bars (partially hidden by the plot markers) are statistically based on a reducted  $\chi^2$  analysis ( $\sim$ 12 K).

direction transverse to the gradient gives a 1D plot of temperature as a function of the position along the flake [Fig. 4(c)]. Fitting these temperature profiles reveals that the (switchable) temperature gradients are 70–90 K/ $\mu$ m (-90 K/ $\mu$ m for left heating, blue line, and 70 K/ $\mu$ m for right heating, red line). The error in temperature, determined from the normally distributed temperatures in the isothermal columns in Fig. 4(b)'s temperature maps, is 20 K.

From the temperature gradient of 80 K/ $\mu$ m and our 20 K temperature uncertainty, we can estimate our spatial resolution  $\sigma_R$  to be 250 nm (slope  $\sim \sigma_T/\sigma_R$ ). This resolution is not limited by the thermometry technique's spatial resolution *per se*, which is determined by (see Ref. [8]) the image pixel size (6 nm) and the plasmon delocalization length ( $\sim$ 2 nm, which is similar to our probe size of 1–2 nm), but by its precision and the temperature gradient's size. Our gradient of 80 K/ $\mu$ m = 8 × 10<sup>5</sup> K/cm is already large by macroscopic standards, but the ideal target for a resolution test would feature a step change in the temperature. Such a step is impossible to arrange and difficult to even approximate, since the thermal conductivities of real materials span only a few orders of magnitude (compare, e.g., electrical conductivities, which span many).

In summary, we apply Raman thermometry and PEET to a  $MoS_2$  flake on a commercial, calibrated MEMS-style TEM heating chip. Ramping the chip temperature from room temperature to 1100 K (according to the chip calibration) gives corresponding Raman and PEET temperature curves that are internally consistent at the few percent level, but that gives values 10% high and 20% low relative to

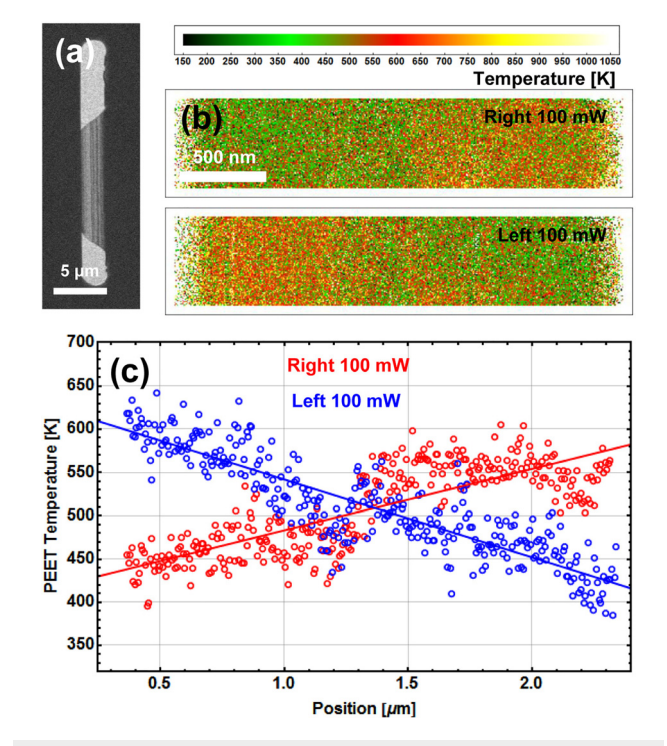


**FIG. 4.** (a) Higher-magnification STEM image of the device of Fig. 1(b), rotated  $90^{\circ}$ , showing the MoS<sub>2</sub> flake spanning the slit in the chip. PEET-derived 2D temperature maps (b) and 1D temperature profiles (c) plotted along the suspended length of a MoS<sub>2</sub> flake. A rectangular ROI is used (long direction across the slit), and the results are averaged in the short direction ( $\sim$ 80 points).

the chip temperature, respectively. These systematic discrepancies highlight the need for more careful studies of the TECs and Raman-peak-frequency temperature coefficients in MoS<sub>2</sub> and other TMDCs. Interpreting the STEM EELS experiment as a measurement of the MoS<sub>2</sub> volume TEC gives  $\alpha_1 = (1.9 \pm 0.1) \times 10^{-5} \; \mathrm{K^{-1}}$  and  $\alpha_2 = (5 \pm 8) \times 10^{-10} \; \mathrm{K^{-2}}$  in the measured temperature range of 300–1100 K. We then used this TEC value to map 70–90 K/ $\mu$ m temperature gradients in a suspended flake of MoS<sub>2</sub> with a submicrometer spatial resolution. The basic procedure reported here, which determines the TEC if unknown and then maps the plasmon energy to determine the temperature, is general and can be most profitably applied in nanostructures made of materials (e.g., many semiconductors) with sharp plasmon resonances and sizable TECs.

See the supplementary material for two figures describing the curve fitting used to determine the plasmon energy, plasmon energy maps at different temperatures, a schematic of the experiment, and images of the connections to the MoS<sub>2</sub> flake. The first supplementary figure shows the plasmon energy maps and characteristics of the fitting, and the second shows an overview of how the Joule heaters are connected to the device.

This research was supported by the National Science Foundation (NSF) Award No. CBET-1905357 (L.S.), NSF Award Nos. DMR-1611036 and DMR-1548924 (B.C.R.), and the Department of Energy (DOE) Award No. DE-FG02-07ER46376 (R.D.) The data were acquired at the University of Southern California's Core Center of Excellence in Nano Imaging (CNI).

## REFERENCES

- <sup>1</sup>D. Jariwala, V. K. Sangwan, L. J. Lauhon, T. J. Marks, and M. C. Hersam, "Emerging device applications for semiconducting two-dimensional transition metal dichalcogenides," ACS Nano 8(2), 1102–1120 (2014).
- <sup>2</sup>S. B. Desai, S. R. Madhvapathy, A. B. Sachid, J. P. Llinas, Q. X. Wang, G. H. Ahn, G. Pitner, M. J. Kim, J. Bokor, C. M. Hu, H. S. P. Wong, and A. Javey, "MoS2 transistors with 1-nanometer gate lengths," Science 354(6308), 99–102 (2016).
- <sup>3</sup>I. Calizo, A. A. Balandin, W. Bao, F. Miao, and C. N. Lau, "Temperature dependence of the Raman spectra of graphene and graphene multilayers," Nano Lett. 7(9), 2645–2649 (2007).
- <sup>4</sup>G. Kucsko, P. C. Maurer, N. Y. Yao, M. Kubo, H. J. Noh, P. K. Lo, H. Park, and M. D. Lukin, "Nanometre-scale thermometry in a living cell," Nature 500(7460), 54–U71 (2013).
- <sup>5</sup>L. Shi, S. Plyasunov, A. Bachtold, P. L. McEuen, and A. Majumdar, "Scanning thermal microscopy of carbon nanotubes using batch-fabricated probes," Appl. Phys. Lett. 77(26), 4295–4297 (2000).
- <sup>6</sup>F. Menges, P. Mensch, H. Schmid, H. Riel, A. Stemmer, and B. Gotsmann, "Temperature mapping of operating nanoscale devices by scanning probe thermometry," Nat. Commun. 7, 10874 (2016).
- <sup>7</sup>F. Könemann, M. Vollmann, F. Menges, I.-Ju. Chen, N. M. Ghazali, T. Yamaguchi, K. Ishibashi, C. Thelander, and B. Gotsmann, "Nanoscale scanning probe thermometry," in 24rd International Workshop on Thermal Investigations of ICs and Systems (THERMINIC) (2018).
- <sup>8</sup>M. Mecklenburg, W. A. Hubbard, E. R. White, R. Dhall, S. B. Cronin, S. Aloni, and B. C. Regan, "Nanoscale temperature mapping in operating microelectronic devices," Science 347(6222), 629–632 (2015).

- <sup>9</sup>M. Mecklenburg, B. Zutter, and B. C. Regan, "Thermometry of silicon nanoparticles," Phys. Rev. Appl. 9(1), 014005 (2018).
- 10 D. Flannigan and D. Cremons, "Direct in situ thermometry: Variations in reciprocal-lattice vectors and challenges with the Debye-Waller effect," Ultramicroscopy 161, 10–16 (2016).
- <sup>11</sup>M. Lagos and P. Baston, "Thermometry with subnanometer resolution in the electron microscope using the principle of detailed balancing," Nano Lett. 18(7), 4556–4563 (2018).
- <sup>12</sup>J. C. Idrobo, A. R. Lupini, T. Feng, R. Unocic, F. Walden, D. Gardiner, T. C. Lovejoy, N. Dellby, S. T. Pantelides, and O. L. Krivanek, "Temperature measurement by a nanoscale electron probe using energy gain and Loss spectroscopy," Phys. Rev. Lett. 120, 095901 (2018).
- <sup>13</sup>L. Mele, S. Konings, P. Dona, F. Evertz, C. Mitterbauer, P. Faber, R. Schamers, and J. R. Jinnschek, "A MEMS-based heating holder for the direct imaging of simultaneous in-situ heating and biasing experiments in scanning/transmission electron microscopes," Microsc. Res. Tech. 79(4), 239–250 (2016).
- 14. G. Eda, G. Fanchini, and M. Chhowalla, "Large-area ultrathin films of reduced graphene oxide as a transparent and flexible electronic material," Nat. Nanotechnol. 3(5), 270–274 (2008).
- <sup>15</sup>H. D. Phan, Y. Kim, J. Lee, R. Liu, Y. Choi, J. H. Cho, and C. Lee, "Ultraclean and direct transfer of a Wafer-scale MoS2 thin film onto a plastic substrate," Adv. Mater. 29(7), 1603928 (2017).
- <sup>16</sup>Z. Li, G. Ezhilarasu, I. Chatzakis, R. Dhall, C. C. Chen, and S. B. Cronin, "Indirect band gap emission by hot electron injection in metal/MoS2 and metal/WSe2 heterojunctions," Nano Lett. 15(6), 3977–3982 (2015).
- <sup>17</sup>N. Poudel, S. J. Liang, D. Choi, B. Y. Hou, L. Shen, H. T. Shi, L. K. Ang, L. Shi, and S. Cronin, "Cross-plane thermoelectric and thermionic transport across AU/h-BN/graphene heterostructures," Sci. Rep. 7, 14148 (2017).
- <sup>18</sup>S. Sahoo, A. P. S. Gaur, M. Ahmadi, M. J. F. Guinel, and R. S. Katiyar, "Temperature-dependent Raman studies and thermal conductivity of few-layer MoS2," J. Phys. Chem. C 117(17), 9042–9047 (2013).
- <sup>19</sup>M. Thripuranthaka, R. V. Kashid, C. S. Rout, and D. J. Late, "Temperature dependent Raman spectroscopy of chemically derived few layer MoS2 and WS2 nanoflakes," Appl. Phys. Lett. **104**(12), 081911 (2014).
- 20 T. Livneh and E. Sterer, "Resonant Raman scattering at exciton states tuned by pressure and temperature in 2H-MoS<sub>2</sub>," Phys. Rev. B 81, 195209 (2010).
- <sup>21</sup>J. A. Wilson and A. D. Yoffe, "Transition metal dichalcogenides discussion and interpretation of observed optical, electrical and structural properties," Adv. Phys. 18(73), 193 (1969).
- <sup>22</sup>H. Abe, M. Terauchi, R. Kuzuo, and M. Tanaka, "Temperature-dependence of the volume-plasmon energy in aluminum," J. Electron Microsc. 41(6), 465–468 (1992).
- <sup>23</sup>G. Meyer, "Uber Die Abhangigkeit Der Charakteristischen Energieverluste Von Temperatur und Streuwinkel," Z. Phys. 148(1), 61–71 (1957).
- 24P. Palanisamy and J. M. Howe, "Melting and supercooling studies in submicron Al particles using valence electron energy-loss spectroscopy in a transmission electron microscope," J. Appl. Phys. 110(2), 024908 (2011).
- <sup>25</sup>Y. C. Ding and B. Xiao, "Thermal expansion tensors, Gruneisen parameters and phonon velocities of bulk MT2 (M = W and Mo; T = S and Se) from first principles calculations," RSC Adv. 5(24), 18391–18400 (2015).
- 26S. H. El-Mahalawy and B. L. Evans, "The thermal expansion of 2H-MoS2, 2H-MoSe2 and 2H-WSe2 between 20 and 800° C," J. Appl. Crystallogr. 9(5), 403–406 (1976).
- <sup>27</sup>R. Murray and B. L. Evans, "The thermal expansion of 2H-MoS<sub>2</sub> and 2H-WSe<sub>2</sub> between 10 and 320 K," J. Appl. Crystallogr. 12, 312–315 (1979).
- 28 C. K. Gan and Y. Y. F. Liu, "Direct calculation of the linear thermal expansion coefficients of MoS<sub>2</sub> via symmetry-preserving deformation," Phys. Rev. B 94, 134303 (2016)
- <sup>29</sup>X. Hu, P. Yasaei, J. Jokisaari, S. Öğüt, A. Salehi-Khojin, and R. F. Klie, "Mapping thermal expansion coefficients in freestanding 2D materials at the nanometer scale," Phys. Rev. Lett. 120, 055902 (2018).
- <sup>30</sup>L. Huang and Z. Zeng, "Roles of mass, structure, and bond strength in the phonon properties and lattice anharmonicity of single-layer Mo and W dichalcogenides," J. Phys. Chem. C 119, 18779–18789 (2015).